Optimization of a Circularly Polarized Conical Beam Microstrip Patch Antenna Array Conformed on a Cylindrical Surface Using HFSS

Probir K. Dhar*

Abstract—When a planar microstrip patch antenna is conformed to any non-planar surface (e.g., aircraft, missiles etc.), the curvature of the host surface affects its design parameters, which in turn affects its radiation performance. Therefore, achieving a target radiation performance with a planar antenna on a non-planar host surface is always a big challenge for an antenna designer. To address this issue, a report on an electromagnetic simulation-based method to optimize a planar-shaped microstrip antenna array conformed to a cylindrical surface is presented here. HFSS was used to investigate the role of different design parameters of the antenna array in the planar and cylindrical planes (for different radius of curvature). Finally, using these simulation observations, the dimensions of the planar antenna conformed to a cylindrical surface (with a radius of curvature of 110 mm) were optimized to achieve a target output performance (in terms of gain, return loss, and VSWR) while retaining its radiation pattern geometry as well as polarization characteristics. A planar 2×2 circularly polarized antenna array with a conical beam pattern from the published literature was used to carry out the current work. After rigorous optimization, return loss < -19 dB, VSWR of 1.807, and as much as 8.135 dBi gain at 2.45 GHz have been achieved. This report should be a useful guide for mounting any planar antenna array on a non-planar host surface. And it will also be helpful to design conformal microstrip antennas for different practical applications.

1. INTRODUCTION

Microstrip patch antennas (MSPAs) have a wide range of applications in the field of mobile communication. A simple microstrip antenna consists of a radiating patch, a dielectric substrate, and a ground plane. The patch and ground plane are normally made of copper. Patches can be of any shape; however, regular shapes are generally used for simplicity in analysis. Microstrip patch antennas radiate primarily because of the fringing fields between the patch edge and the ground plane. The dielectric constant of the substrate plays a controlling role in the fringe field and loss tangent. The choice of substrate depends on the desired radiation performance of the antenna [1]. MSPAs are smaller in size, light in weight, have a low fabrication cost, and are easy to integrate with microwave circuits [2, 3]. In spite of having such advantages, microstrip antennas are limited by their inherent low efficiency, low gain, and narrow bandwidth nature, which require judicious design approaches to overcome [4, 5].

Sometimes it is desired to mount the antenna structure on a host surface that may not be planar but rather cylindrical, conical, or spherical, such as the surfaces of aircraft, missiles, satellites, ships, vehicles, and base stations. The electrical and mechanical characteristics of conformal MSPAs and their arrays make them a suitable choice for installation on non-planar structures [6, 7]. These radiators

can sometimes be integrated into non-planar structures. In existing literature, the performance of microstrip patch antenna arrays conformed to curved (cylindrical) host surfaces, and their application in the telecommunication field can be found as an interesting research topic [8–10].

An analytical study reveals that the effect on the radiation pattern is negligible for small curvature cylinders, whereas large curvatures might considerably deform the antenna radiation pattern [11]. Planar microstrip patch antenna arrays, when being conformed to curved surfaces, suffer from the change in their radiation performance because antenna parameters are affected due to the effect of curvature on the fringing field. Again, in the case of a conformal antenna structure, the shape of the radiation pattern is also affected by the feed structure [12]. Hence, designing a planar antenna array with a simple feed structure will be a better option to achieve the desired radiation pattern when being conformed on a non-planar host surface. Hence, the main challenge of a planar antenna array conformed to a non-planar host surface is to counter the effect of host surface curvature on its radiation performance. Some disadvantages of antennas on conformal plane include narrow band and mutual coupling between basic elements [13–15]. As a result, optimizing the planar antenna dimension when it is wrapped on any specific curved plane becomes necessary to retain the desired characteristics of the planar radiator.

In this work, an existing planar antenna design with known performance was chosen from the available literature [16, 17]. The antenna with a single-feed structure and subsequent patch geometry modification (to achieve CP) was much easier to implement in a conformal structure. The detailed description of the planar antenna is mentioned in Section 2. These structural advantages made this antenna a better candidate to be considered for this present work. Here, the performance of this MSPA both on planar and cylindrical surfaces (with different radius of curvature) has been investigated using full wave simulation software, Ansoft HFSS 2015 [18]. Finally, the antenna, conformed to a cylindrical surface with a radius of curvature of 110 mm, was optimized to generate a target output (in terms of return loss, voltage standing wave ratio (VSWR), and gain) and to retain its radiation pattern geometry and polarization characteristics. Section 2 contains a brief description of the design as well as parametric dependencies. In the present work, the considered planar array antenna wrapped to the specified cylindrical surface was optimized to achieve the best return loss, VSWR, and gain at the centre frequency of 2.45 GHz and simulated to retain the desired conical beam radiation pattern and circular polarization with a low axial ratio using full wave simulation software, Ansoft HFSS 2015 [18]. After rigorous optimization at 2.45 GHz, a return loss < -19 dB, a VSWR of 1.807, and as much as 8.135 dBi gain have been achieved with the retention of the circular polarization characteristics and conical beam pattern on the host cylindrical plane with a radius of curvature of 110 mm. The optimized antenna is omnidirectional in the circumferential direction and has a beam about 30° in the elevation direction, i.e., it can have gain only at the elevation angle of 30°. Such a beam pattern makes it suitable to be mounted on the curved surface on the roof of car for short-range low power Wireless Sensor Network applications such as Bluetooth and Wi-Fi.

2. ARRAY ANTENNA DESIGN

The schematic layout of the considered stripline-fed conical-beam CP microstrip patch antenna [17] is shown in Figure 1. It consists of four square patches with stripline feed. Each rectangular patch with a rectangular slot in the centre has its diagonally opposite corners chamfered (for circular polarization (CP) generation). All four feedlines meet at the central point of the array structure. For the present antenna, air (relative permittivity $\epsilon_r = 1$, dielectric loss tangent $\tan \delta = 0.001$) has been considered as the substrate. Since the lower dielectric constant of air can yield a wider bandwidth. A 10 mm air gap has been considered between the patch and the ground plane.

In a rectangle-shaped microstrip patch antenna, the resonant frequency depends on the length of the patch antenna (L_p) while the width (W_p) determines the resonance impedance. Hence, the dimensions of the square patch antenna are to be determined judiciously to achieve the desired impedance matching at the desired resonance frequency. The dielectric substrate thickness (H_{sub}) decides the impedance bandwidth. Circular polarization can be achieved by two different methods: first, by feeding a square patch on two adjacent sides with a phase difference of 90° and second, by using a single feed to one side of a square patch that has been chamfered in two diagonally opposite corners. In the later case, the
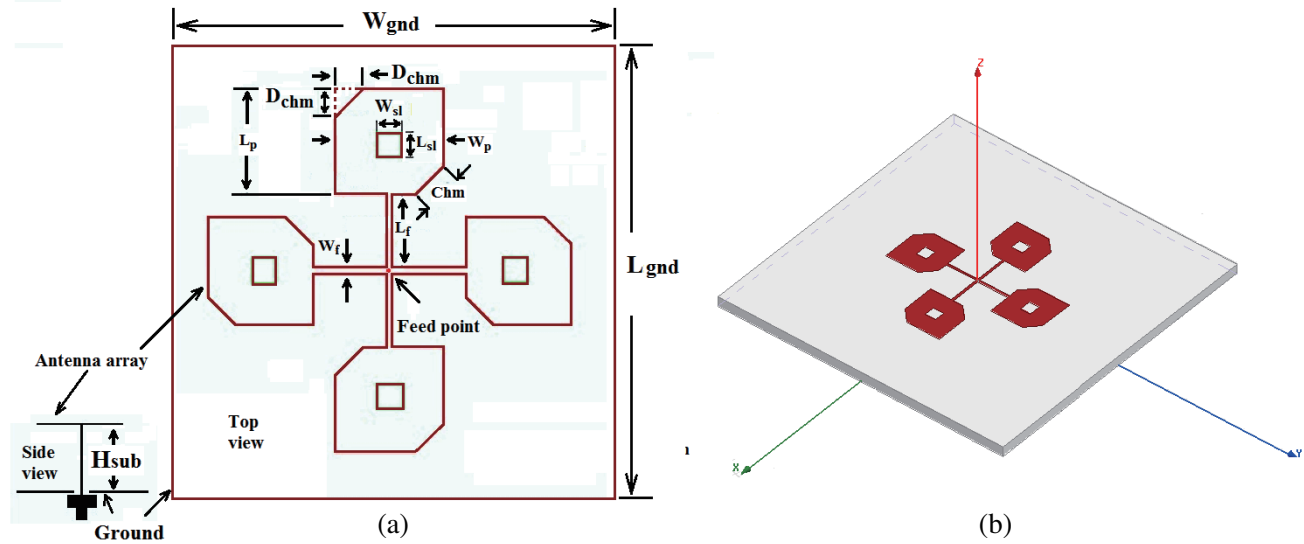
Figure 1. (a) AutoCAD-generated schematic diagram of the antenna array; (b) HFSS implemented model.

chamfered corners result in a variance in frequencies with 90° phase shift [19]. In the present design, each single feed rectangular patch of the 2 × 2 MSPA array has a rectangle-shaped slot of dimension $W_{sl} \times L_{sp}$ square unit at the centre. All dimensions are as considered in [17] and tabulated in Table 1.

Table 1. Dimension of circularly polarized microstrip patch antenna.

Design parameters	Variables	Dimensions (in mm)	
		As mentioned in [17]	After optimization
Substrate width	W_{sub}	300	300
Substrate length	L_{sub}	300	300
Ground width	W_{gnd}	300	300
Ground length	L_{gnd}	300	300
Substrate height	H_{sub}	10	8.8
Depth of chamfering	D_{chm}	12	11.2
Chamfer length	Chm	16.97	15.83
Patch width	W_p	46	47.2
Patch length	L_p	45	46.6
Feed width	W_f	2.5	3.70
Feed length	L_f	31.25	31.4
Slot width	W_{sl}	11	12
Slot length	L_{sl}	10	11.6
Connector height	H_{con}	7.2	7.2
Outer radius of connector	Rad_{out}	1.75	1.75
Inner radius of connector	Rad_{in}	0.5	0.5

3. DESIGN ANALYSIS

Figure 2(a) represents the geometry of a typical single-fed circularly polarized microstrip square patch antenna. A patch with a single feed typically radiates linear polarization; to radiate CP, two orthogonal patch modes with equal magnitude and in-phase quadrature need to be induced. This can be achieved by slightly perturbing a patch at the right feed-related locations. The truncated sizes of the corners and modes of circularly polarized signals are given by the following equations:

$$\Delta s/S = 1/2Q \tag{1}$$
$$f_a = f_r + \Delta f'_a = f_r[1 - (2\Delta s)/S] \tag{2}$$
$$f_b = f_r + \Delta f'_b = f_r \tag{3}$$

where $\Delta s = \Delta s_1 + \Delta s_2$ represents the total sum of the two perturbation areas of each patch, and S and Q denote the patch area and quality factor of the patch, respectively. The patch area $S = L_p \times W_p$. The depth of chamfering (D_{chm}) determines the axial ratio (AR). In the present design, D_{chm} is kept equal along the X and Y directions, i.e., $a = b = 12\,\text{mm}$. Hence, $\Delta s = 12^2$. Again, f_a and f_b denote the new resonant frequencies generated by the chamfered corners. $\Delta f'_a$ and $\Delta f'_b$ represent the shift in resonant frequencies for the generation of two orthogonally degenerate modes due to perturbation segments [20].
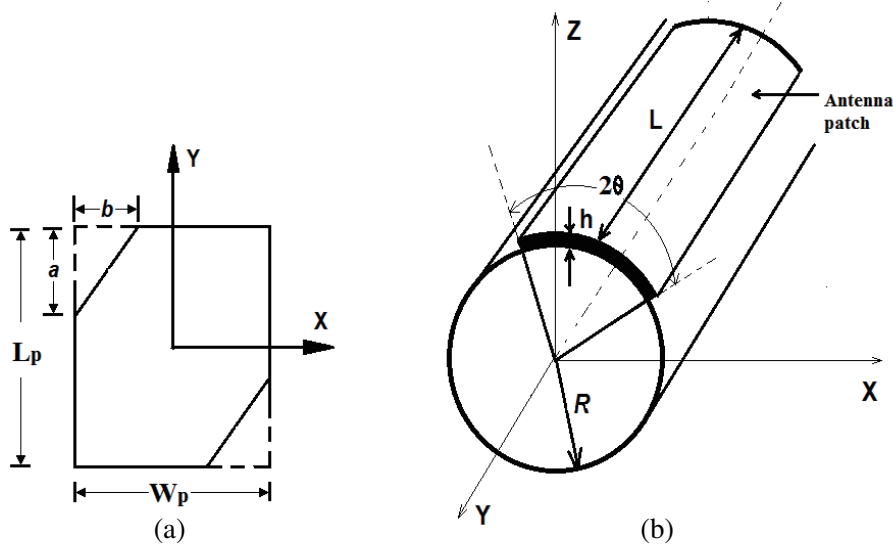

Figure 2. Configuration of (a) single-fed circularly polarized rectangular microstrip antenna and (b) cylindrical rectangular patch antenna.

The dimensions of the patch are determined by solving the following sets of Equations (4) to (7) of dielectric constant $(\mathbb{C}_r)$, resonant frequency (f_r), and height of substrate (H_{sub}) [6]:

The width of the patch

$$(W_p) = \frac{c}{2f_r}\sqrt{\frac{2}{\varepsilon_r + 1}} \tag{4}$$

Effective dielectric constant of the substrate

$$(\epsilon_{\textit{eff}}) = \left(\frac{\varepsilon_r + 1}{2}\right) + \left(\frac{\varepsilon_r - 1}{2}\right)\left(1 + 12\frac{H_{sub}}{W_p}\right)^{-1/2} \tag{5}$$

Extended incremental length of the patch

$$(\Delta L_p) = 0.412 H_{sub}\frac{(\varepsilon_{\textit{eff}} + 0.3)\left(\dfrac{W_p}{H_{sub}} + 0.264\right)}{(\varepsilon_{\textit{eff}} - 0.258)\left(\dfrac{W_p}{H_{sub}} + 0.8\right)} \tag{6}$$

Actual Length of the patch $(L_p) = \lambda/2 - 2\Delta L_p$

$$\text{Or,} \quad L_p = \frac{1}{2 f_r \sqrt{\varepsilon_{eff}} \sqrt{\mu_0 \varepsilon_0}} - 2\Delta L_p \tag{7}$$

In Figure 3, the HFSS simulated return loss plot has been compared with the CST simulated and measured return loss plot of Zhou et al., 2009 [17]. Here, the HFSS-generated plot is in close agreement with the CST-simulated and measured plot of [17]. The antenna dimensions considered here are those of Zhou et al., 2009 as shown in Table 1.
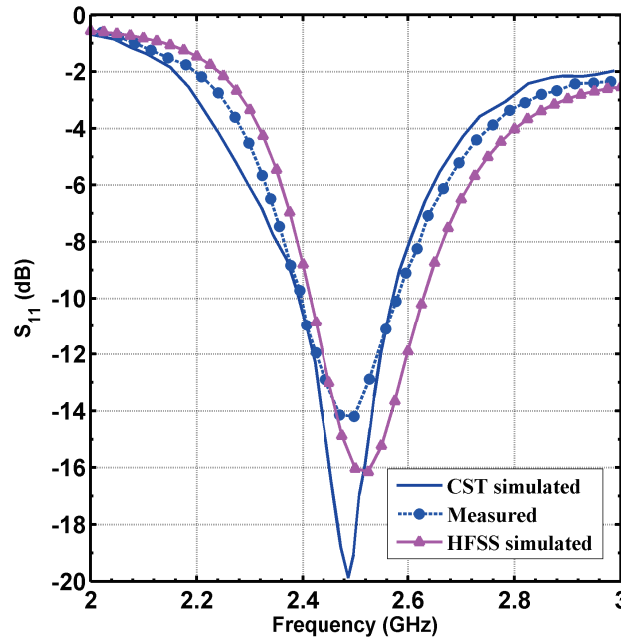

Figure 3. Comparison of the HFSS simulated return loss, CST simulated return loss [17] and measured return loss [17] plots (with the antenna dimensions as followed in [17]).

The E-field distribution due to the array of patches is shown in Figure 4. All the patches are excited in identical phase. The rotation of the fields ensures right hand circularly polarized (RHCP) excitations.

3.1. Parametric Analysis

In this section, parameter analysis is presented to illustrate the considered antenna array design. Considering the complexity of the antenna design, only several parameters critical for optimizing a good AR and return loss performance, such as the Depth of chamfer (D_{chm}), patch width (W_p), patch length (L_p), feed width (W_f), feed length (L_f), slot width (W_{sl}), slot length (L_{sl}), and substrate height (H_{sub}), are investigated in this paper. Variation in the length of the design parameters has been observed to have an effect on output performance in terms of return loss and axial ratio. Only one design parameter is changed each time, while the others are fixed. All the values considered are those as described in [17] and shown in Table 1.

Figure 5.1 depicts the effects of substrate height (H_{sub}) variation on the S_{11} and AR. The reason for this result is that the thickness of the substrate would affect not only the input impedance of the proposed antenna but also the amplitude of the two orthogonal electric fields, which in turn changes the S_{11} and AR of the antenna array, respectively. The effects of chamfer length (Chm) on S_{11} and AR are presented in Figure 5.2. As shown, when the depth of chamfer (D_{chm}) is increased, impedance bandwidth and AR bandwidth both become wider, and the AR bandwidth moves to the higher frequency band with a simultaneous increase in AR values. Figure 5.3 illustrates that the variation in the slot
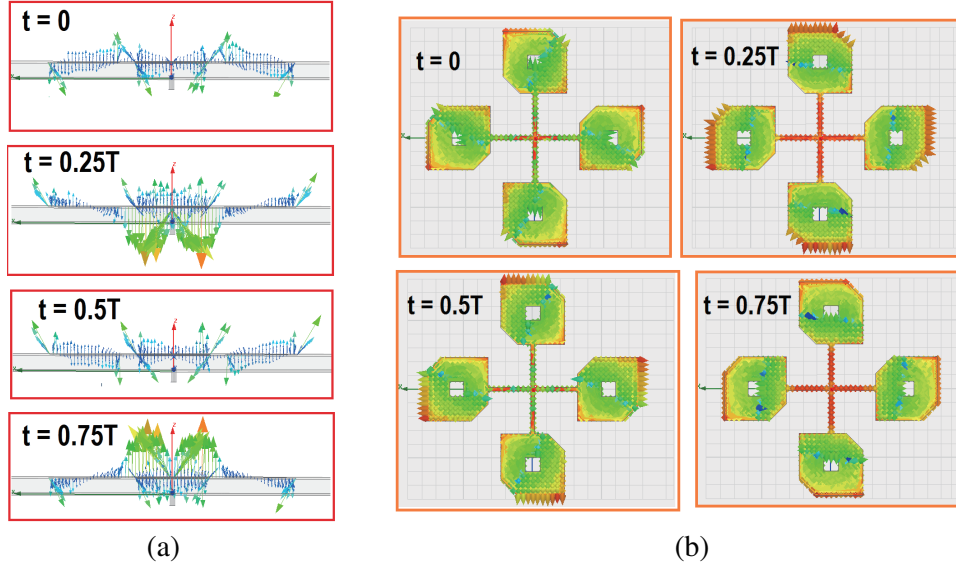
Figure 4. (a) Side view and (b) Top view of E-field distribution of planar antenna geometry in HFSS.

width (W_{sl}) has little effect on the AR bandwidth, but has a considerable effect on the impedance matching. The plot shows that as W_{sl} increases, the resonant frequency shifts to a lower frequency band. Figure 5.4 illustrates that the variation in the slot length (L_{sl}) has little or no effect on the impedance matching. However, AR bandwidth undergoes a minor left shift as L_{sl} increases. Figure 5.5 illustrates that the variation in the feed width (W_f) has little effect on the AR bandwidth but a great effect on the impedance matching. The plot shows that as W_f increases, S_{11} improves, and resonant frequency shifts towards the lower frequency band. The sizes of the patch width (Wp) and patch length (Lp) are studied to better illustrate the effect of patch width (Wp) and patch length (Lp) on the performances of the proposed antenna, as shown in Figures 5.6 and 5.7, respectively. In Figure 5.6, only the size of the patch width (W_p) is changed in steps of 1 mm, while other antenna dimensions as considered in [17] are kept constant as mentioned in Table 1. It has been observed that when the size of the patch width (W_p) is increased, the impedance bandwidth decreases. Resonance frequency was found to be shifted towards a higher frequency band, whereas AR ratio bandwidth was found to shift towards a lower frequency band. However, in Figure 5.7, plots are generated when only the size of the patch length (L_p) is changed in steps of 1 mm while other antenna dimensions as considered in [17] are kept constant as mentioned in Table 1. It has been observed that when the size of the patch length (L_p) is increased, the resonance frequency shifts towards the lower frequency band. However, AR bandwidth remains almost unaltered.

3.2. Effect of Radius of Curvature

The effect of mutual coupling in a planar antenna array can be observed when the space between the antenna elements is changed. This change in mutual coupling is reflected in the input impedances of the array [13–15]. For conformal structures, curvature also affects the mutual coupling that induces currents on nearby antenna elements and scatters into the far field. As a result, the radiation pattern and input impedance change considerably [21, 23]. This has been demonstrated in Figure 6, where the magnitudes of the real and imaginary parts of the impedance are found to change as a function of frequency for different values of the radius of curvature of the host surface.

In literature, numerous works have been reported to explore the effect of curvature on the performance of a conformal rectangular patch antenna [23]. For the sake of simplicity, they have all made some assumptions, e.g., in a conformal rectangular microstrip antenna, the curvature does not affect the effective dielectric constant and the extension on the length, i.e., permittivity (ϵ) and permeability (μ) were considered to remain constant (i.e., homogeneous medium filling the cavity) and real (i.e., no

dielectric losses), i.e., conformally mounted microstrip antennas may be considered planar. In 1983, Krowne [10], in an attempt to assess the validity of this commonly used assumption, used numerical analysis to demonstrate the effect of the curvature of the host surface on the resonant frequency of a
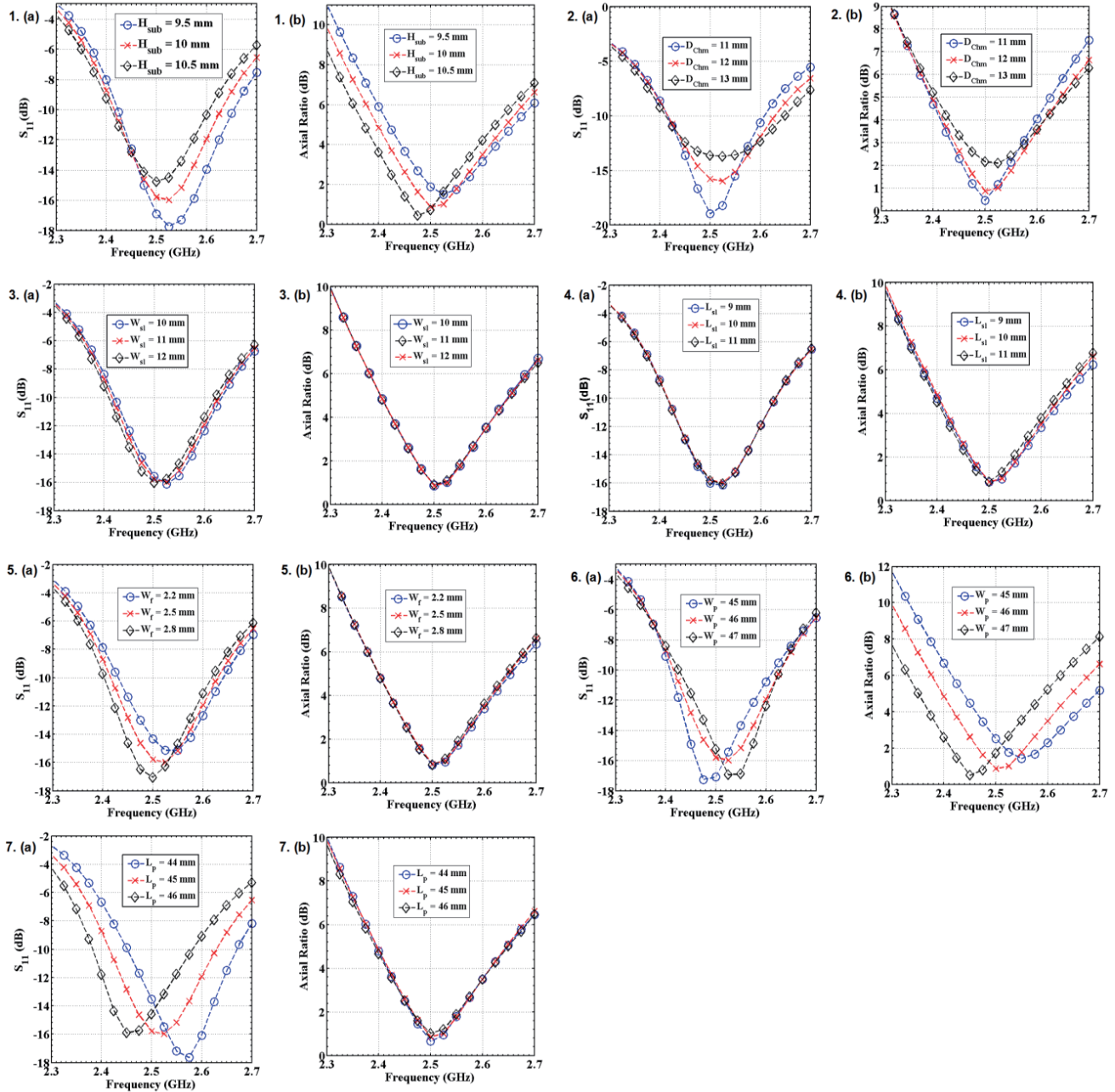

Figure 5. Effects of different design parameters (with dimensions as considered in [17]) on Return loss and Axial ratio. 1. (a) and (b) show return loss and axial ratio plots for various substrate height (H_{sub}) values. 2. (a) and (b) show return loss and axial ratio plots for various depths of chamfer (D_{chm}). 3. (a) and (b) depict Return loss and Axial ratio plots for different values of slot width (W_{sl}). 4. (a) and (b) depict Return loss and Axial ratio for different values of slot length (L_{sl}). 5. (a) and (b) depict Return loss and Axial ratio with different values of feed width (W_f). 6. (a) and (b) depict Return loss and Axial ratio with different values of patch width (W_p) and 7. (a) and (b) depict Return loss and Axial ratio with different values of patch length (L_p).
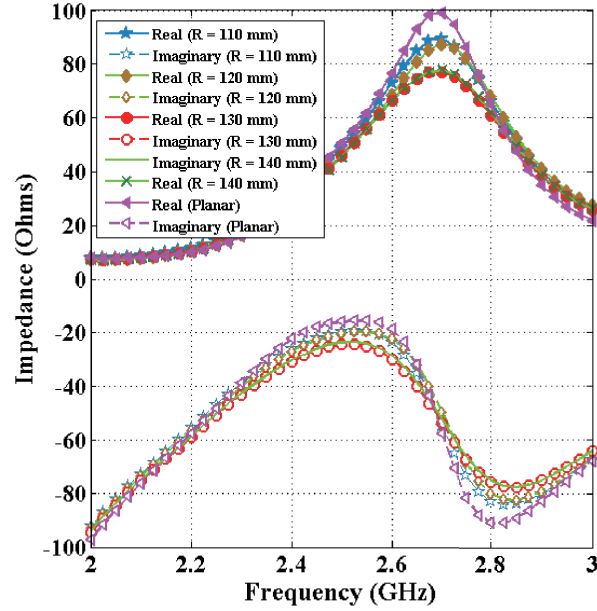
Figure 6. Effect of various radius of curvature (R) on the input impedance of the microstrip antenna array on a cylindrical surface (with dimensions as considered in [17]).

rectangular microstrip antenna, and the resonant frequency (f_r) was calculated as follows:

$$(f_r) = \frac{1}{2\pi\sqrt{\varepsilon\mu}}\sqrt{\left(\frac{m\pi}{2\theta R}\right)^2 + \left(\frac{l\pi}{L}\right)^2} \tag{8}$$

where R is the radius of the cylindrical host surface, L the length of the patch antenna, and 2θ the angle subtended by the width of the patch at the centre of the cylinder, as shown in Figure 2(b). ε and μ represent the electric permittivity and magnetic permeability, respectively. In this work, the eigenvalue equations for resonant frequencies (f_r) over a range of dielectric substrate thickness h were solved both for planar and conformal structures, and the numerical values of eigen frequencies (f) for both cases were compared to assess the effect of curvature on resonant frequency. It was found that for a substrate with dielectric thickness equal to one tenth of the radius of curvature, f_r change is less than 5 percent. Specifically, the results show that this assumption is valid for h which is small in comparison to the surface curvature. Finally, it was determined that the exact effect of curvature on f_r is dependent on the antenna parameters involved [10]. In the present work, in an attempt to investigate the above behavior, simulation exercises were carried out with the considered planar MSPA array conformed on a cylindrical host surface (Figures 6–10). The radius of curvature (R) of the cylindrical host surface was varied in steps of 10 mm with an initial value of 110 mm, keeping the antenna dimensions constant as considered in [17]. Simulation results show that the output plot (e.g., return loss, radiation pattern, gain, etc.) of a conformal antenna deforms from that of its planar form for every change in the radius of curvature value of the host surface. A shift in resonance has been observed as the radius of curvature value changes. This necessitates the need for a further simulation run to optimize the dimension of the present antenna array to achieve its target output performance on a conformal surface for any given radius of curvature (R). The model was implemented in [18] for different radii of curvatures (R) of the host cylindrical surface. Rigorous simulation exercises were carried out to investigate the effect of the curvature of the host cylindrical surface on return loss, gain, radiation pattern, and axial ratio, and the observations are reported as follows.

In Figure 7(a), return loss plots of the antenna with the dimension as mentioned in Zhou et al., 2009 [17] are generated for the antenna with planar and conformal structures with different radii of curvature. Simulation plots show a minor shift in the resonance frequency of the conformal antenna towards higher frequencies compared to the planar one. This finding corroborates the observation of
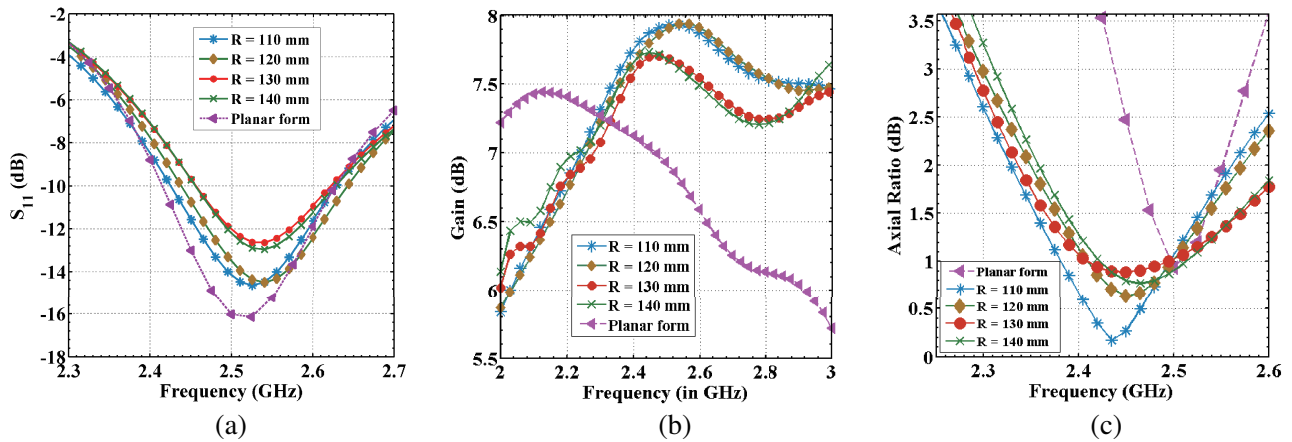
Figure 7. Effect of various radius of curvature (R) of the cylindrical surface on antenna radiation parameters as a function of frequency. (a) Return loss. (b) Axial ratio and (c) Gain of the antenna. Antenna dimensions are as considered in [17].

Kolev, 2003, where a small conformal microstrip GPS patch antenna was designed (using cavity model and transmission line model analysis followed by successive electromagnetic simulation using FEKO), and the experimental results were matched with the simulation ones [22]. Similar observations have been reported by Elrashidi et al., 2012 [23]. However, it has been observed by Elleithy et al., 2011 that the resonance frequency remains almost constant with curvature [24]. Figure 7(b) shows that in the case of a planar antenna array, the gain is always below 7.5 dBi, and after 2.12 GHz it shows a downward trend as frequency increases. However, for conformal structures (with radii of curvature of 110 mm, 120 mm, 130 mm, and 140 mm), the gain increases with frequency and maintains gain flatness above 7 dBi for a wide range. Figure 7(c) shows that when the dimension of the radius of curvature was increased stepwise, the AR ratio bandwidth was found to get modified accordingly.

In Figure 8, three pattern cuts, at constant φ, i.e., $\varphi = 0°$, $\varphi = 30°$, and $\varphi = 45°$ along with their cross, were taken due to the symmetrical geometry of the proposed antenna. According to the
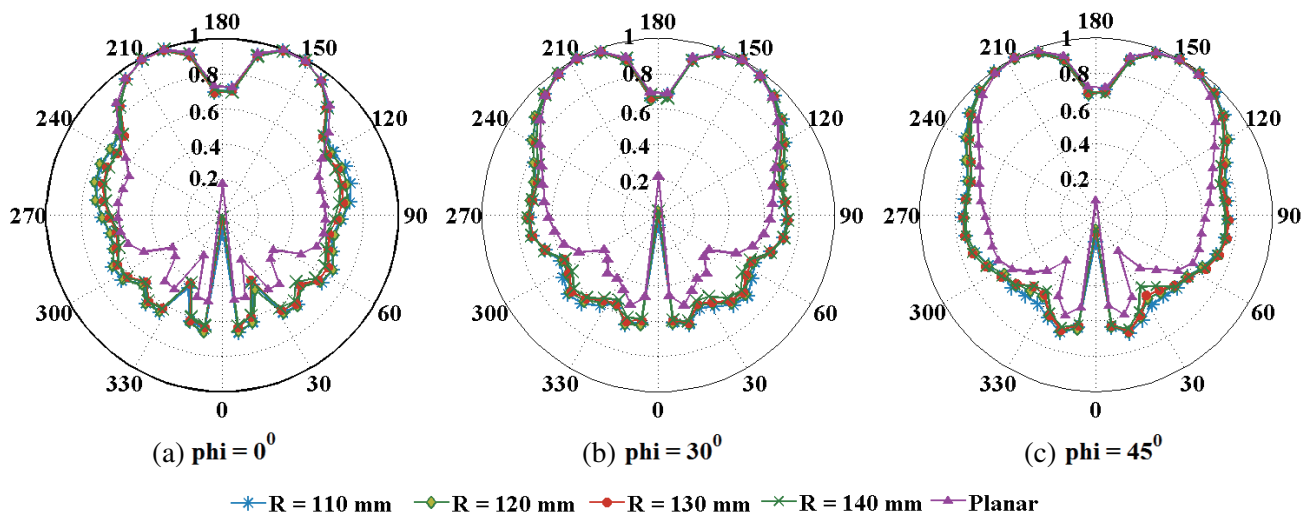

Figure 8. HFSS simulated radiation pattern at 2.45 GHz for planar and conformal antenna structures with different radius of curvatures (R) for (a) $phi = 0°$ cut, (b) $phi = 30°$ cut, and (c) $phi = 45°$ cut with antenna dimension as considered in [17].

simulation results, the radiation pattern is affected by the radius of curvature of the cylindrical surface and produces higher side-lobes and a wider beamwidth when being conformed. This finding corroborates the experimental findings of You et al., 2007 [25].

4. ANTENNA ARRAY OPTIMIZATION RESULTS AND COMPARISON

The planar MSPA antenna implemented in the HFSS simulator was wrapped on a cylindrical host surface with $R = 110$ mm. Figure 9 depicts 3D views of the HFSS-implemented conformal microstrip patch antenna array with antenna dimensions as stated by Zhou et al., 2009 [17].
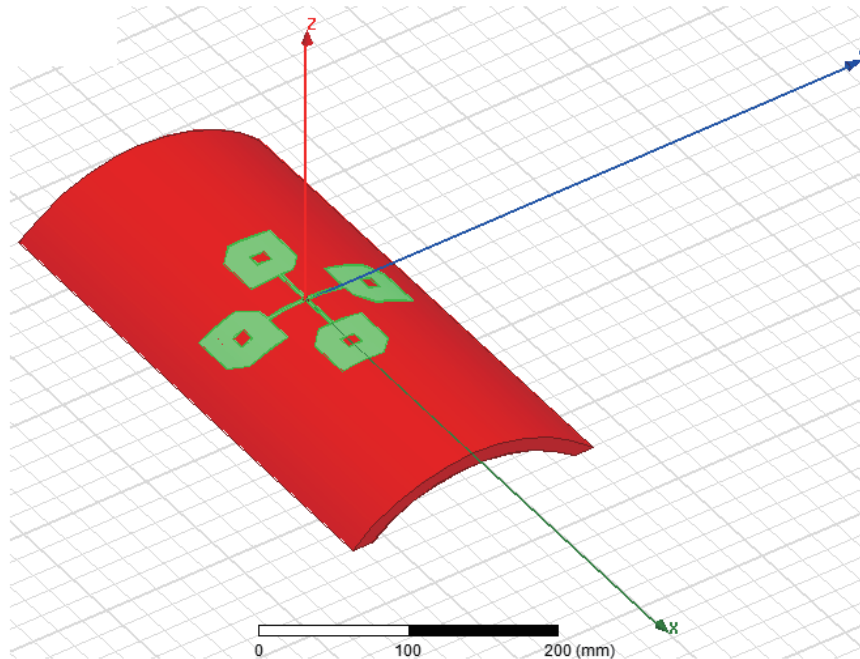

Figure 9. HFSS generated 3D model of the conformal CP antenna structure.

It was observed that the planar antenna array, when being conformed on a cylindrical surface with $R = 110$ mm and simulated at 2.45 GHz, VSWR and return loss deteriorated from 3.9501 to 4.6901 and -13.011 dB to -11.580 dB respectively (Table 2). However, simulation results show that in direction $\varphi = 45°$ and $\theta = 42°$, the axial ratio was improved from 2.47 dB to 0.87 dB, and the gain was improved from 7.04 to 7.87 dBi (Table 2). Finally, dimensions of the square patch, height of the substrate, dimensions of the slot, depth of chamfering are optimized through successive simulations using HFSS [18] to achieve the target output performance of the antenna array on the host cylindrical surface of the given radius of curvature. The values of the optimized dimensions are presented in Table 1. Figure 10 depicts plots for real and imaginary parts of input impedance for an antenna in planar and conformal form with a radius of curvature of 110 mm. The plot shows that at 2.45 GHz the real part of the input impedance has a peak value of almost 60 Ω, and the imaginary part is almost zero. The value of 2.45 GHz represents the resonance frequency for the conformal antenna with a radius of curvature of 110 mm.

Figure 11(a) compares the return loss of the antenna with the dimensions mentioned in [17] to that of the antenna with optimized dimensions (Table 1). In both cases, plots are generated for the antenna with planar and conformal structures for a radius of curvature (R) of 110 mm. Simulation plots show that in the case of a conformal antenna structure with optimized dimensions, a better return loss is achieved at the resonance frequency (2.45 GHz) compared to the planar one. In Figure 11(b), the gain versus frequency plots of the antenna with the dimension as mentioned in [17] are compared with
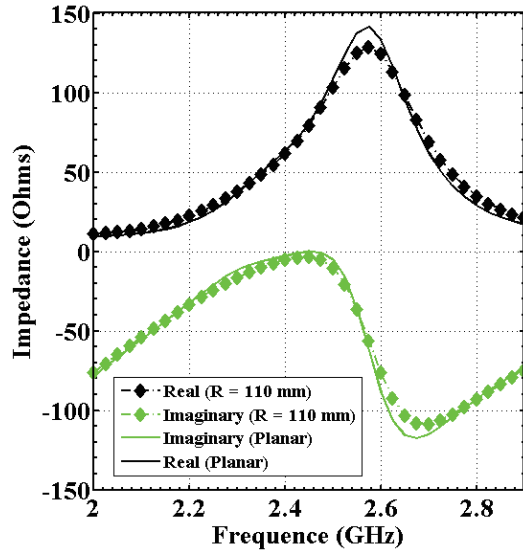
Figure 10. Simulated input impedance against frequency plot of the antenna in planar and conformal form (with a radius of curvature (R) of 110 mm) after optimization.
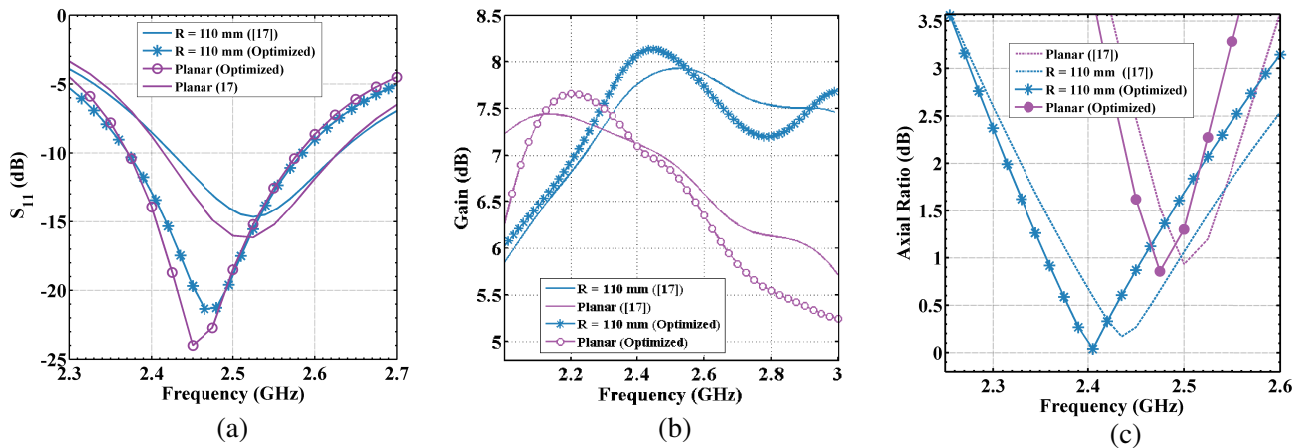

Figure 11. Comparison of the (a) Return loss, (b) Gain (for $\varphi = 45°$ and $\theta = 42°$ at 2.45 GHz) and (c) Axial ratio (for $\varphi = 45°$ and $\theta = 42°$ at 2.45 GHz) of the antenna in planar and conformal form (with a radius of curvature (R) of 110 mm) before (with dimension as considered in [17]) and after optimization. Optimized antenna dimensions are depicted in Table 1.

those of the antenna with the optimized dimension (Table 1). In both cases, plots are generated for the antenna with planar and conformal structures with different radii of curvatures. Simulation plots show that in the case of the conformal antenna structure with optimized dimensions, better gain is achieved (greater than 8 dBi) at resonance frequency (2.45 GHz) than the antenna without optimized dimensions. A simulated axial ratio (in the direction $\varphi = 45°$ and $\theta = 42°$) comparison of planar and conformal array antennas (with a given radius of curvature of 110 mm) before (i.e., with dimensions as followed in [17]) and after optimization (i.e., with dimensions as mentioned in Table 1) is shown in Figure 11(c). The graph shows that in the case of an antenna with optimized dimensions (Table 1), the axial ratio at 2.45 GHz is almost equal to 0.87 dB. In general, for an ideal CP antenna, AR should be 0 dB. However, practical antennas are elliptically polarized. It indicates that circular polarization is achieved in the above direction. Simulation shows that after optimization, the axial ratio bandwidth of conformal antennas is increased to 12.73%, compared to 5.58% for the initial planar antenna array (dimensions

as considered in [17]). It is also observed that after optimization for the conformal structure, the AR bandwidth for AR $< 2\,$dB overlaps with the impedance bandwidth for $|S_{11}| < -10\,$dB in the range of $2.38\,$GHz to $2.52\,$GHz in the above-mentioned direction [26], i.e., the overlap bandwidth obtained after optimization is 5.71%. Prior to optimization, the AR bandwidth for AR $< 2\,$dB overlaps with the impedance bandwidth for $|S_{11}| < -10\,$dB in the range of $2.45\,$GHz to $2.55\,$GHz, i.e., the overlap bandwidth obtained was 4.39%. Therefore, a 1.32% increase in overlap bandwidth has been achieved through optimization.

In Figure 12, three pattern cuts, at constant φ, i.e., (i) $\varphi = 0°$, (ii) $\varphi = 30°$, and (iii) $\varphi = 45°$ were taken of the antenna for (i) planar structure (with dimension as mentioned in Table 1) and (ii) conformal
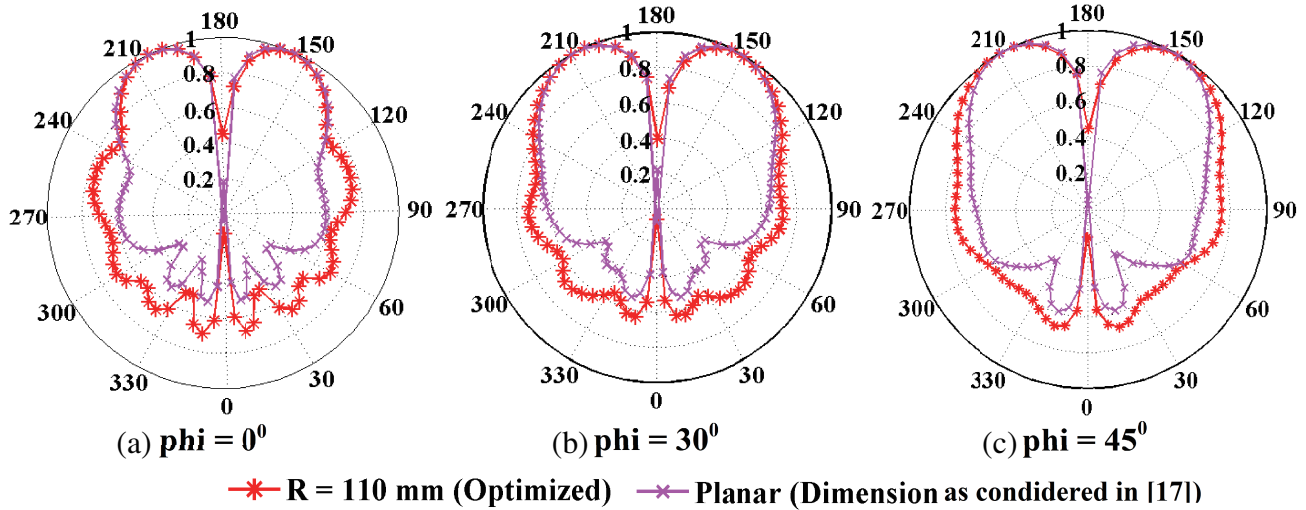

Figure 12. Comparison between the simulated radiation pattern (at $2.45\,$GHz) of planar antenna structures (dimensions as considered in [17]) and optimized conformal ($R = 110\,$mm) antenna structures (dimensions as mentioned in Table 1) for (a) $phi = 0°$ cut (b) $phi = 30°$ cut and (c) $phi = 45°$ cut.
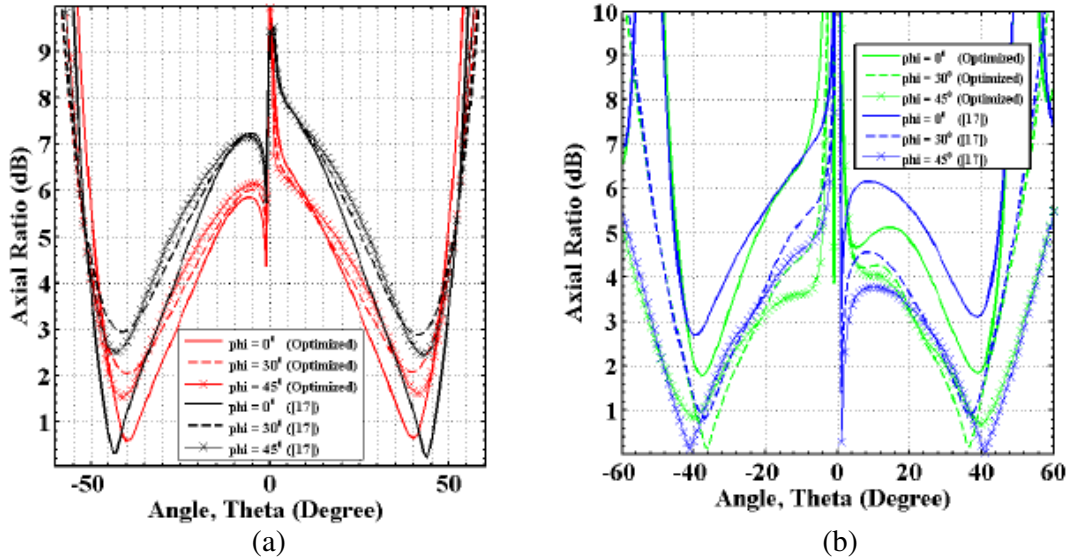

Figure 13. Simulated axial ratio versus elevation angle (theta) plot before (dimension as followed in [17]) and after optimization (dimensions as mentioned in Table 1) with three different phi cuts $\varphi = 0°$, $\varphi = 30°$ and $\varphi = 45°$ plot at $2.45\,$GHz for (a) planar array antenna (b) conformal array antenna with radius of curvature $110\,$mm.

structure with optimized dimension (as mentioned in Table 1). The simulation results revealed that the main beam of the radiation pattern conformal antenna remained nearly unchanged after optimization while producing higher side-lobes. This finding corroborates with experimental findings of You et al., 2007 [25].

Figure 13(a) and Figure 13(b) illustrate before and after optimization axial ratios against elevation angle (theta) plots at 2.45 GHz for the antenna in planar and conformal forms (with a radius of curvature (R) of 110 mm). Here, like in radiation patterns (Figure 12), the same three vertical planes, $\varphi = 0°$, $\varphi = 30°$, and $\varphi = 45°$, are considered. The results show that in both cases, axial ratios remain less than 2 dB for elevation angles (θ) around peak gain. So we conclude that the designed antennas achieved circular polarization in the above three vertical planes.

Simulated co-polarization and cross-polarization patterns at 2.45 GHz (center frequency of the simulated impedance bandwidth) for left hand circular polarization (LHCP) and RHCP reception for planar and conformal antenna arrays (for $R = 110$ mm) are shown in Figure 14. It clearly indicates that in the case of conformal structure (for $R = 110$ mm) after optimization RHCP has been achieved with cross-polarization discrimination about 18 dB at $\theta = 30°$ and 18 dB at $\theta = -30°$.

(a)   (b)
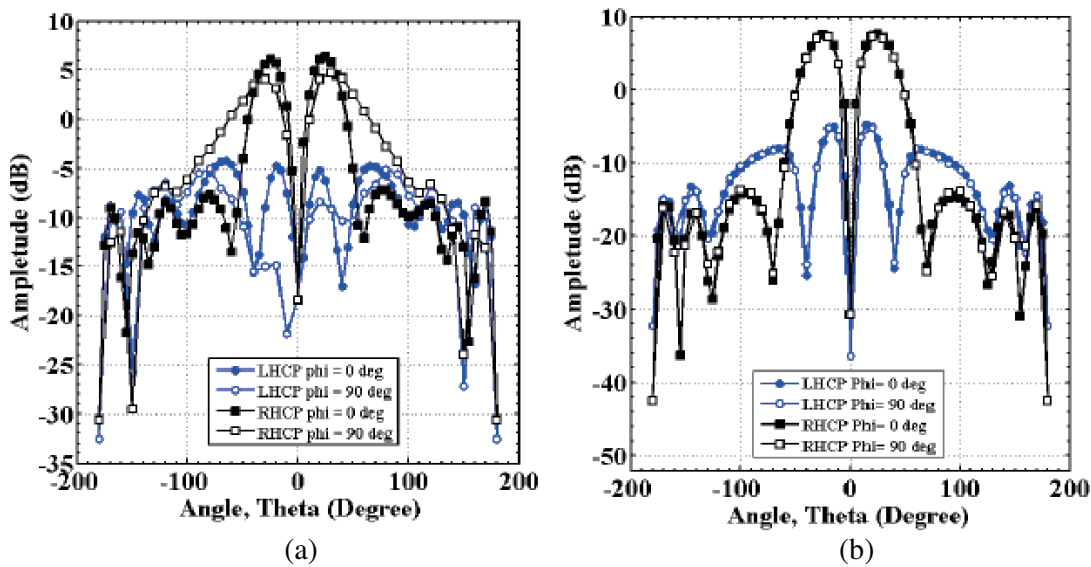
Figure 14. Simulated radiation patterns of the antenna at 2.45 GHz (LHCP and RHCP reception) after optimization (dimensions as mentioned in Table 1) for (a) planar array antenna (b) conformal array antenna with radius of curvature 110 mm.

5. DISCUSSION

In Table 2, simulation data at different frequency points on cylindrical surfaces with different radii of curvature are also included for a better understanding of the variation in antenna radiation performance as a function of frequency and host surface curvature. Here the optimized antenna's (i.e., with dimensions as depicted in Table 1) performance is compared with the existing literature antenna's (i.e., with dimensions as depicted in Table 1) performance. It shows that the planar antenna conformed to a cylindrical plane with a given radius of curvature of 110 mm after optimization attains better results in most categories and comparable results in the remainder. Table 2 shows that at 2.45 GHz, for a cylindrical plane with a radius of curvature of 110 mm, the VSWR and return loss values were increased when the antenna was conformed but improved after optimization. Table 2 also shows that at this frequency, the gain and beamwidth of the conformal antenna were also increased after optimization. Table 2 shows that for conformal antenna AR is less than 3 dB over the frequency range 2.3–2.5 GHz, i.e., the circular polarization property is retained within this range.

Table 2. Comparison of radiation performance between the antenna with dimension as followed by Zhou et al., 2009 (as mentioned in Table 1) and optimized dimension (as mentioned in Table 1) both in planar and conformal form.

F†	Antenna structure		Dimension dimension as depicted in **Table 1**					Optimized dimension as depicted in **Table 1**				
			3dB Beamwidth (in deg) at Φ =		Gain (in dBi)	AR (in dB)	ρ§	Γ (in dB)	3dB Beamwidth (in deg) at Φ =		Gain (in dBi)	AR (in dB)	ρ	Γ (in dB)
			30⁰ cut	120⁰ cut	at (Φ = 45⁰, θ = 42⁰)				30⁰ cut	120⁰ cut	at (Φ = 45⁰, θ = 42⁰)			

F†	Antenna structure		3dB BW 30⁰ cut	120⁰ cut	Gain (dBi)	AR (dB)	ρ§	Γ (dB)	3dB BW 30⁰ cut	120⁰ cut	Gain (dBi)	AR (dB)	ρ	Γ (dB)
2.2	Conformal													
	R$	110	40	40	6.8	4.77	19.853	-1.7729	36	40	6.92	5.05	17.760	-2.2609
		120	34	33	6.72	5.11	20.759	-1.5964	36	41	6.98	5.449	17.623	-2.2972
		130	40	40	6.82	5.13	21.365	-1.4881	35	43	6.54	4.45	18.584	-2.0543
		140	36	40	6.96	5.74	21.579	-1.4518	34	40	7.14	5.58	18.421	-2.0935
	Planar		32	31	7.4	15.3	21.521	-1.4614	35	34	7.6	15.576	19.807	-1.7825
2.3	Conformal													
	R	110	32	42	7.31	2.60	13.111	-3.9041	34	39	7.557	2.37	10.603	-5.2821
		120	34	40	7.23	2.98	14.033	-3.4996	35	40	7.589	2.908	10.322	-5.4671
		130	32	40	7.08	2.78	14.361	-3.3667	35	41	7.355	2.536	11.491	-4.7413
		140	36	40	7.2	3.27	14.512	-3.3071	33	40	7.556	3.03	11.257	-4.8773
	Planar		31	31	7.27	9.7	14.392	-3.3542	35	34	7.5	9.69	11.960	-4.4804
2.4	Conformal													
	R	110	33	41	7.8	0.68	6.8648	-8.5006	33	39	8.07	0.063	4.0220	-12.861
		120	34	40	7.66	1.14	7.5388	-7.7734	34	43	7.93	0.5798	3.6943	-13.576
		130	33	41	7.58	1.07	8.2023	-7.1320	33	41	7.844	1.45	4.6171	-11.711
		140	40	48	7.66	1.28	8.2492	-7.0892	32	35	7.89	1.444	4.4389	-12.038
	Planar		32	32	7.12	4.65	6.6141	-8.7935	31	33	7.10	3.998	3.5437	-13.927
2.45	Conformal													
	R	110	32	32	7.87	0.87	4.6901	-11.580	34	39	8.135	0.87	1.807	-19.690
		120	37	40	7.8	0.64	5.1870	-10.752	33	41	7.93	0.559	1.721	-20.108
		130	32	42	7.7	0.89	5.9049	-9.6984	32	42	7.86	1.60	2.384	-17.306
		140	39	43	7.73	0.798	5.8871	-9.7227	32	41	7.84	1.37	2.302	-17.605
	Planar		32	32	7.04	2.47	3.9501	-13.011	32	32	6.97	1.618	1.097	-24.004
2.5	Conformal													
	R	110	34	38	7.9	1.06	3.4371	-14.185	32	38	8.064	1.68	1.9784	-18.908
		120	34	37	7.9	1.01	3.7116	-13.536	34	38	7.867	1.55	2.2703	-17.725
		130	32	38	7.7	1.02	4.4316	-12.051	31	39	7.705	1.75	2.3966	-17.260
		140	40	44	7.69	0.90	4.3339	-12.237	30	40	7.62	1.50	2.4009	-17.245
	Planar		31	31	6.93	0.93	2.7674	-16.029	31	31	6.84	1.30	2.0734	-18.504
2.6	Conformal													
	R	110	33	37	7.87	2.54	4.6540	-11645	32	36	7.74	3.14	6.4185	-9.0313
		120	33	35	7.9	2.36	4.2513	-12.397	31	35	7.548	3.307	6.6773	-8.7184
		130	32	35	7.55	1.78	5.0683	-10.941	32	34	7.209	2.33	5.9718	-9.6078
		140	38	45	7.5	1.84	4.8993	-11.220	31	33	7.03	1.50	6.0520	-9.5007
	Planar		30	30	6.59	3.58	4.5184	-11.89	30	30	6.35	5.22	11.960	-8.644

† Radius of curvature (in mm).

$ Frequency (in GHz).

§ VSWR

A brief investigation of the proposed and related antenna arrays is depicted in Table 3. Table 3 describes four conformal CP antennas with conical beam patterns [27–30]. Compared with other antennas, the proposed structure shows higher gain. Although the antennas in [27, 28] have wider impedance bandwidth and AR bandwidth, the gains still need to be improved. Again, the antenna in [30] has a higher impedance bandwidth, but its gain and AR bandwidth are lower than the proposed antenna. However, the substrate integrated waveguide (SIW) antenna presented in [29] shows lower impedance bandwidth, AR bandwidth, and gain than the proposed antenna. Considering the simple structure, low profile, high gain, and good AR bandwidth together, simulation shows that the conical-beam CP antenna has good performance compared to those antennas shown in Table 3, which makes it a good candidate for wireless communication systems.

Table 3. Comparison among proposed and related antenna arrays.

Ref.	Type	Polarization	Conformal	Beam pattern	S_{11}, (dB %)	AR, (dB %)	Peak gain, (dBic)
[27]	microstrip	CP	Yes	Conical beam	4.9–6.5 (28)	5.8–6.7 (14.4)	4.9
[28]	microstrip	CP	Yes	Conical beam	5.04–6.12 (19.4)	4.9–5.32 (25.3)	6.5
[29]	SIW	CP	Yes	Conical beam	17.6–18.15 (3.1)	17.6–18.25 (3.6)	7.1
[30]	microstrip	CP	Yes	Conical beam	5.35–6.75 (23.1)	5.95–6.55 (9.6)	7.45
This work	microstrip	CP	Yes	Conical beam	2.37–2.58 (8.48)	2.28–2.59 (12.73)	8.135

Recently published articles on 10 elements and 18 elements array antennas for 5G MIMO smartphone reported simulated individual antenna elements gain greater than 5.9 dBi and the measured antenna elements gain greater than 5.3 dBi [31, 32]. The proposed four elements antenna array, with its higher gain (8.135 dBi), low AR (0.87 dB), and good AR ratio bandwidth, can also be a better candidate for 5G applications. Due to its higher axial ratio (2.28–2.59 GHz, 12.73%), this antenna can be used for polarization diversity where propagation conditions are unknown, and its conical pattern can be utilized to reduce co-channel interference. However, simulation shows that the present conformal antenna is workable in the ISM band only and suffers from low impedance bandwidth (2.37–2.58 (8.48%)). A suitable wideband technique (e.g., the aperture coupled technique) can be incorporated into the present design to achieve broad impedance bandwidth [33–39]. Once necessary design modifications make it wideband, the present design can be a better candidate for a future 5G communication network (i.e., long term evolution (LTE) band 42 (3.4–3.6 GHz), LTE band 43 (3.6–3.8 GHz), and LTE band 46 (5.15–5.925 GHz)). Again, the current antenna requires size reduction to fit in a 5G smartphone where, unlike the previously mentioned 5G MIMO antenna placement, this conical beam antenna can be placed in the centre of the PCB with other electronic circuitry placed on the PCB's edge or side frame.

6. CONCLUSION

The conformal antenna after optimization on a cylindrical surface (with a radius of curvature of 110 mm) shows improvements in gain, axial ratio, return loss, and VSWR compared to planar form. At a resonating frequency of 2.45 GHz, a good axial ratio (0.87 dB), a higher gain (8.135 dB) (highest among the other antennas listed in Table 3), a VSWR less than 2, and a conical beam pattern with beamwidths of 34° and 39° at $phi = 30°$ and 120° cut are obtained. The simulated result shows that an increase in AR bandwidth (5.58% to 12.73%) for AR < 3 dB has been achieved when planar antenna was conformed and optimized. In comparison to a planar antenna array, a 1.32% increase in overlap bandwidth (axial ratio bandwidth for AR < 2 dB and impedance bandwidth for $|S_{11}| < -10$ dB) was obtained in optimized conformal antenna. Due to higher axial ratio bandwidth (2.28–2.59 GHz (12.73%)) for AR < 3 dB this antenna can be used for polarization diversity where propagation conditions are unknown. Again, this antenna with a conical pattern can be used in a wireless sensor network (WSN) to reduce co-channel interference. The higher side lobe of the radiation pattern of a conformal antenna can be reduced by further optimization or by applying different side lobe reduction techniques. The current study described in this communication should serve as a useful guide for conforming any planar antenna array on a non-planar host surface, as well as for designing conformal microstrip antennas in a variety of practical applications. In conclusion, the design of this optimized conformal antenna shows a good performance, is suitable for the wireless system, and can also be a good candidate for future 5G communication after subsequent design modifications make it wideband.

ACKNOWLEDGMENT

REFERENCES

1. James, J. R. and P. S. Hall, *Handbook of Microstrip Antennas*, London, UK, Peter Peregrinus, 1989.
2. Wong, K. L., *Design of Nonplanar Microstrip Antennas and Transmission Lines*, John Wiley & Sons, Inc., New York, ISBN: 978-0-471-46390-0, 1999.
3. Josefsson, L. and P. Persson, *Conformal Array Antenna Theory and Design*, John Wiley & Sons, Inc., Hoboken, New Jersey, 2006.
4. Carver, K. R. and J. W. Mink, "Microstrip antenna technology," *IEEE Trans. Antennas Propag.*, Vol. 29, No. 1, 2–24, Jan. 1981.
5. Richard, W. F., Y. T. Lo, and D. D. Harrison, "An improved theory for microstrip antennas and applications," *IEEE Trans. Antennas Propag.*, Vol. 29, No. 1, 38–46, Jan. 1981.
6. Balanis, C. A., *Antenna Theory Analysis and Design*, 2nd Edition, John Wiley & Sons, Inc., New York, 1997.
7. Garg, R., P. Bhartia, I. Bhal, and A. Ittipiboon, *Microstrip Antenna Design Handbook*, 1st Edition, Norwood, Artech House, 2000.
8. Rostan, F., G. Gottwald, and W. Wiesbeck, "Design and performance of con-formal microstrip patch arrays on cylindrical surfaces," *Proc. EuMC*, 1756–1761, Cannes, 1994.
9. Godara, L. C., "Applications of antenna arrays to mobile communications, Part II: Beam-forming, and direction-of-arrival considerations," *Proc. IEEE*, Vol. 85, No. 8, 1195–1245, Aug. 1997.
10. Krowne, C. M., "Cylindrical-rectangular microstrip antenna," *IEEE Trans. Antennas Propag.*, Vol. 31, No. 1, 194–199, Jan. 1983.
11. Thomas, W., R. C. Hall, and D. I. Wu, "Effects of curvature on fabrication of wraparound antennas," *IEEE International Symposium on Antenna and Propagation Society*, Vol. 3, 1512–1515, Jul. 1997.
12. Ferreira, D. B., C. B. de Paula, and D. C. Nascimento, "Design techniques for conformal microstrip antennas and their arrays," *Advancement in Microstrip Antennas with Recent Applications*, Mar. 2013, doi: 10.5772/53019.
13. Jedlicka, R., M. Toe, and K. Carver, "Measured mutual coupling between microstrip antennas," *IEEE Trans. Antennas Propag.*, Vol. 29, 147–149, Jan. 1981.
14. Penard, E. and J. Danial, "Mutual coupling between microstrip antennas," *Electron. Lett.*, Vol. 18, No. 14, 605–607, Jul. 1982.
15. Pozar, D., "Input impedance and mutual coupling of rectangular microstrip antennas," *IEEE Trans. Antennas Propag.*, Vol. 30, 1191–1196, Nov. 1982.
16. Abd-Alhameed, R. A., N. J. McEwan, E. M. Ibrahim, and P. S. Excell, "A new design of horizontally-polarised and dual-polarized uniplanar antennas for HIPERLAN," *IEEE Trans. Antennas Propag.*, Vol. 51, 229–237, 2003.
17. Zhou, D., R. A. Abd-Alhameed, C. H. See, N. J. McEwan, and P. S. Excell., "New circularly-polarised conical-beam microstrip patch antenna array for short-range communication systems," *Microwave And Optical Technology Letters*, Vol. 51, No. 1, Jan. 2009, doi 10.1002/mop.
18. Ansoft, High Frequency Structure Simulator (HFSS), v.15.
19. Haneishi, M. and S. Yoshida, "A design method of circularly polarised rectangular microstrip antenna by one-point feed," *Microstrip Antenna Design*, K. C. Gupta and A. Benalla (eds.), 313–321, Artech House, Norwood, MA, 1988.

20. Cairo, L. and T. Kahan, *Variational Techniques in Electromagnetism*, Blackie and Son, London, UK, 1965.

21. Warnick, K. and M. Jensen, "Effects of mutual coupling on interference mitigation with a focal plane array," *IEEE Trans. Antennas Propag.*, Vol. 53, No. 8, 2490–2498, Aug. 2005.

22. Kolev, N. Z., "Design of a microstip conform GPS patch antenna," *IEEE 17th International Conference on Applied Electromagnetic and Communications*, 201–204, 2003.

23. Elrashidi, A., K. Elleithy, and H. Bajwa, "Performance analysis of a microstrip printed antenna conformed on cylindrical body at resonance frequency 4.6 GHz for TM_{01} mode," *Procedia Computer Science, 9th International Conference on Mobile Web Information Systems*, Vol. 10, 775–784, 2012, doi: 10.1016/j.procs.2012.06.099.

24. Elleithy, K., A. Elrashidi, and H. Bajwa, "Conformal microstrip printed antenna," *ASEE Northeast Section Conference, University of Hartford*, Connecticut, 2011.

25. You, C., W. Hwang, and M. Tenteris, "Impact behavior and radiation performance of a structurally integrated antenna array conformed around cylindrical bodies," *IEEE International Symp. Antennas and Propag. Soc.*, 3844–3847, Jun. 2007.

26. Wei, H., H. Yejun, L. Zhang, S. W. Wong, W. Li, and A. Boag, "A low-profile circularly polarized conical-beam antenna with wide overlap bandwidth," *Hindawi, Wireless Communications and Mobile Computing*, Vol. 2021, Article ID 6648887, 11 pages, doi.org/10.1155/2021/6648887.

27. Lin, W. and H. Wong, "Circularly polarized conical-beam antenna with wide bandwidth and low profile," *IEEE Trans. Antennas Propag.*, Vol. 62, No. 12, 5974–5982, 2014.

28. Yu, D., S.-X. Gong, Y.-T. Wan, et al., "Wideband conical-beam circularly polarized microstrip antenna for large ground plane," *IEEE Trans. Antennas Propag.*, Vol. 63, No. 10, 4614–4619, 2015.

29. Guan, D., Y. Zhang, Z. Qian, et al., "Compact circular polarised SIW array antenna with high gain and conical-beam," *Electron. Lett.*, Vol. 51, No. 24, 1962–1964, 2015.

30. Xu, H., J. Zhou, K. Zhou, et al., "Low-profile circularly polarised patch antenna with high gain and conical beam," *IET Microw. Antennas Propag.*, Vol. 12, No. 7, 1191–1195, 2018.

31. Jaglan, N., S. D. Gupta, and M. S. Sharawi, "18 element massive mimo/diversity 5G smartphones antenna design," *IEEE Access*, Vol. 2, 533–545, 2021, doi: 10.1109/OJAP.2021.3074290.

32. Jaglan, N., S. D. Gupta, B. K. Kanaujia, and M. S. Sharawi, "10 element sub-6-GHz multi-band double-T based MIMO antenna system for 5G smartphones," *IEEE Access*, Vol. 9, 118662–118672, 2021, doi: 10.1109/ACCESS.2021.3107625.

33. Vlasits, T., E. Korolkiewicz, A. Sambell, and B. Robinson, "Performance of a cross-aperture coupled single feed circularly polarized patch antenna," *Electron Lett.*, Vol. 32, No. 7, 612–613, Mar. 1996.

34. Huang, C., J. Wu, and K. Wong, "Cross-slot-coupled microstrip antenna and dielectric resonator antenna for circular polarization," *IEEE Trans. Antennas Propag.*, Vol. 47, No. 4, 605–609, 1999.

35. Huang, C., J. Wu, and K. Wong, "Slot-coupled microstrip antenna for broadband circular polarization," *Electron Lett.*, Vol. 34, No. 9, 835–836, 1998.

36. Adrian, A., "Dual aperture-coupled microstrip antenna for dual or circular polarization," *Electron Lett.*, Vol. 23, 1226–1227, 1987.

37. Karmakar, N. C. and M. E. Bialkowski, "Circularly polarized aperture coupled circular microstrip patch antennas for L-band applications," *IEEE Trans. Antennas Propag.*, Vol. 47, 933–940, 1999.

38. Pozar, D. M. and S. M. Duffy, "A dual-band circularly polarized aperture-coupled stacked microstrip antenna for global positioning satellite," *IEEE Trans. Antennas Propag.*, Vol. 45, 1618–1625, 1997.

39. Targonski, S. D. and D. M. Pozar, "Design of wideband circularly polarized microstrip antennas," *IEEE Trans. Antennas Propag.*, Vol. 41, 214–220, 1993.